Part 3B

Accretion Plasma diagnostics - Theory

Chair: Gary Schmidt

https://doi.org/10.1017/S0252921100002098 Published online by Cambridge University Press

IAU Colloquium 190 on Magnetic Cataclysmic Variables
ASP Conference Series, Vol. 315, 2004
Sonja Vrielmann & Mark Cropper, eds.

Radiation-hydrodynamic Models of the Accretion Spots in Magnetic Cataclysmic Variables

K. Beuermann

Universitäts-Sternwarte Göttingen, Geismarlandstr. 11, D-37083 Göttingen, Germany

Abstract. The structure of the near-polar accretion spots on accreting magnetic white dwarfs has been studied theoretically and observationally in numerous papers over the last decade. Detailed treatments are available for the regime of low mass flux, usually termed the bombardment case, and for higher mass fluxes which create a strong shock standing above the photosphere of the white dwarf. No general treatment is so far available for the case of shocks buried deep in the photosphere. I review the theoretical foundations, present some applications of theory, and discuss in short the open questions which still need to be addressed.

1. Introduction

Observational evidence indicates that the near-polar accretion regions on the white dwarfs at least in some magnetic CVs (MCVs) are highly structured, displaying rapid fluctuations of the mass flux both in the spatial coordinates and in time. Since information of their structure is lacking, a look at well-studied cases of magnetic accretion in the solar system may be inspiring: (i) Jupiter's auroral oval displays substantial structure in its UV emission as observed with the Hubble Space Telescope, and (ii) the Earth's aurora shows narrow striations which extend along field lines and indicate different densities in adjacent flux tubes. Although the physics is different, similar structures *may* exist in MCVs.

Present models of MCV accretion spots are not sufficiently sophisticated to account for such structure. They assume a spatially constant mass flux across the column and are respresentative rather of an individual subcolumn than of the accretion region as a whole. The radiative interaction between individual subcolumns represents a complication which is usually avoided. This neglect may be justified in the optically thin case, but represents a severe restriction if the column is optically thick. In this review, I will summarize the efforts made so far in understanding the properties of accretion columns with special emphasis on the solution of the coupled hydrodynamic and radiative transfer equations.

2. The Accretion Scenario

Figure 1a schematically shows the pole cap of the magnetic accreting white dwarf in a polar. The accretion column is fed by a mass flux $\dot{m} = \rho_o v_o$ (cgs unit $\mathrm{g\,cm^{-2}s^{-1}}$) with ρ_o the density and v_o the value of the free-fall velocity $v_{\rm ff}$ at the

https://doi.org/10.1017/S0252921100002098 Published online by Cambridge University Press

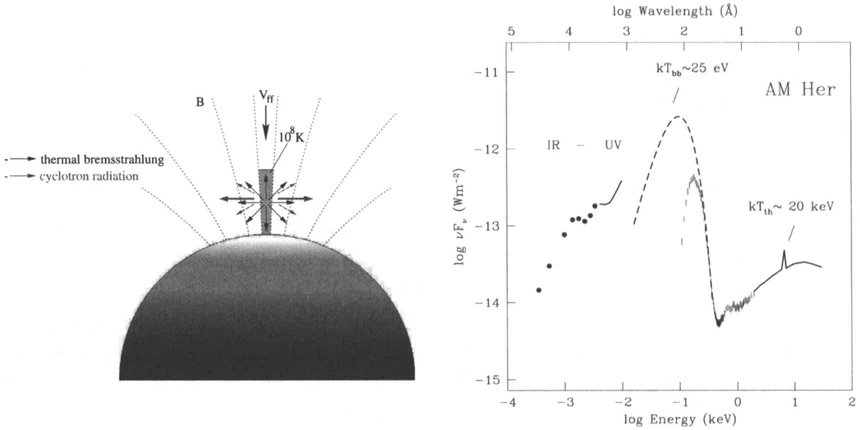

Figure 1. *(a) Left:* Schematic diagram of a (tall) accretion region on the white dwarf (from Gänsicke, priv. comm.). *(b) Right:* Overall spectral energy distribution of the prototype polar AM Herculis at orbital phase $\phi \simeq 0.4$. The dots represent the UBVRIJHK fluxes, the soft X-ray spectrum is from the April 1991 ROSAT observation, and the IUE UV and the HEAO-1 hard X-ray spectrum are shown by solid lines. The dashed line represents the unabsorbed soft X-ray (quasi-)blackbody spectrum.

shock front. The size of the accretion spot depends on the coupling processes in the L_1-point and in the magnetosphere of the white dwarf, while the stand-off distance of the shock front, $h \simeq \frac{1}{4} v_o t_{cool}$ with t_{cool} the cooling time scale, depends on the emission process, i.e. on ρ_o, the electron temperature T_e, and the magnetic field strength B. Depending on the parameters, the emission region in MCVs is either tall (as shown in Fig. 1) or pill-box shaped (i.e. smaller than wide) and the dominant emission process is either hard X-ray bremsstrahlung or IR/optical cyclotron emission. Reprocessing in the atmosphere of the white dwarf produces, in addition, soft X-ray emission from the immediate surrounding of the impact region and UV emission from a wider irradiated area.

The fact that some polars are dominated by soft X-ray emission has been discussed in the literature for some 20 years and dubbed the "soft X-ray problem". In the original model by Lamb & Masters (1979) and King & Lasota (1979), the white dwarf was assumed to intercept $\lesssim 50\%$ of the emission, i.e. the non-reflected fraction of the downward flux, and re-radiate it as soft X-rays. Kuipers & Pringle (1982) effectively solved the mystery of the intense soft X-ray emission by noting that dense blobs of matter would penetrate the photosphere and the subsequent optically thick radiative transfer would reprocess all emissions into quasi-blackbody soft X-rays (see alo Frank et al. 1988).

As an example, Figure 1b displays the overall spectral energy distribution of the prototype polar AM Herculis at an orbital phase at which near-maximum cyclotron and X-ray emission is seen. The spectral energy distribution nicely displays the expected components: (i) cyclotron emission at infrared and optical wavelengths; (ii) the heated polar cap of the irradiated white dwarf in the UV longward of the Lyman edge; (iii) an intense soft X-ray component; and (iv) a hard X-ray bremsstrahlung (+ emission line) component. The companion star and the unheated fraction of the white dwarf are comparatively faint light sources. All accretion-induced emissions fluctuate in time. E.g., the soft X-ray flux of AM Herculis in its high state displays statistically relevant variations down to a time scale of 100 ms, as shown by ROSAT PSPC observations (during the orbital dip when most of the accretion spot is self-eclipsed). This time scale corresponds to density fluctuations in the free-falling pre-shock accretion flow on length scales as short as 10^8 cm. An earlier interpretation of the EXOSAT soft X-ray light curve of AM Her (Hameury & King 1988) suggested already that many such intependent subcolumns are present at any time. For simplicity, most models disregard the inhomogeneities in the pre-shock flow in space and time.

For sufficiently high mass flux, a standing shock separates the infalling matter from the shocked plasma which slowly cools and finally settles onto the white dwarf. An analytic solution for the structure of an optically thin postshock flow cooling by bremsstrahlung was given by Aizu (1973). If the flow is optically thick, which is always the case for cyclotron emission in the fundamental, the solution becomes much more complicated because the radiative transfer has to be treated simultaneously with the hydrodynamics (Woelk & Beuermann 1996).

3. Bombardment solution

In a hydrodynamic shock, the ions are stopped by Coulomb collisions and the shock thickness equals about one ion mean free path. A special situation arises if cooling is so strong that the randomized energy can be radiated by the electrons within that scale length, i.e., effectively "on the spot". In this case, an *extended* post-shock cooling flow does not exist and the concept of a discontinuity separating two regimes of the flow is no longer appropriate. The whole flow has now collapsed to a width which corresponds to the shock thickness and effectively can be described as a hot corona forming part of the white dwarf atmosphere. This mode is referred to as the bombardment solution.

The required efficient cooling for this case can be provided by cyclotron radiation in a strong magnetic field which causes the electron temperature to stay far below the Rankine-Hugoniot temperature $T_{\rm sh}$ of the shock solution. Originally suggested by Kuijpers & Pringle (1982), this case was rigorously solved by Woelk & Beuermann (1992). They treated the ion collisional energy loss by means of statistical plasma physics and simultaneously accounted for the losses of the electrons by a fully frequency-dependent and angle-dependent radiative transfer in a plane-parallel heated atmosphere. The solution predicts a peak electron temperature which increases as $kT_{\rm e} \propto \dot{m}^{0.42}$ (Woelk & Beuermann 1993, see also Fischer & Beuermann 2001) and equals 1 keV for $\dot{m} \simeq 0.01\,{\rm g\,cm^{-2}s^{-1}}$, $B \simeq 30\,{\rm MG}$, and a white dwarf mass of $0.6\,{\rm M_\odot}$. Such low temperatures are observed in AM Her stars with very low accretion rates (Schwope this conference) and suggest that the predicted temperatures are roughly correct. The solution becomes invalid when $T_{\rm e}$ approaches the Rankine-Hugoniot temperature with increasing $\dot{m}$.

4. Radiation-hydrodynamics

For $\dot{m} \gtrsim 0.1\,\mathrm{g\,cm^{-2}s^{-1}}$, the post-shock plasma flow and the radiative transfer have to be treated simultaneously. The only feasible approach is a fluid description which does not allow to resolve the shock front, however. There is no simple connection between such an approach and the kinetic description of the bombardment solution. Nevertheless, we find that the fluid approach for low $\dot{m}$ recovers some important apects of the bombardment case.

4.1. The Equations

The general case assumes a two-fluid plasma and allows for different temperatures $T_{\rm i,e}$ and bulk velocities $v_{\rm i,e}$ of ions and electrons. At the high densities in MCV shocks, Coulomb collisions will assure $\boldsymbol{v}_{\rm i} = \boldsymbol{v}_{\rm e} \equiv \boldsymbol{v}$, except perhaps within the (unresolved) shock front. A two-fluid treatment may then proceed with a single equation of motion which contains the total pressure, i.e. the sum of ion pressure $P_{\rm i}$ and electron pressure $P_{\rm e}$. The skalar pressure and the temperature are related by $P_{\rm i,e} = n_{\rm i,e}kT_{\rm i,e}$ (with $n_{\rm i}$ and $n_{\rm e}$ the particle densities of ions and electrons), which assumes that the particle distributions are isotropic and Maxwellian. Cyclotron losses could, in fact, produce an anisotropic electron distribution function, but the optical depth in the fundamental harmonic is so large that radiative transfer causes the temperatures perpendicular and parallel to the magnetic field to agree closely, except very near the surface of the emission volume (Zhelezniakov 1983). For simplicity, we assume a hydrogen plasma in which $n_{\rm i} = n_{\rm e}$ and the mean molecular weight is $\mu = 1/2$.

The hydrodynamic equations include the continuity equation, the equation of motion, and the energy equations for ions and electrons, which describe the conservation of mass, momentum, and energy, respectively:

$$\frac{d\rho}{dt} + \rho(\nabla\cdot\boldsymbol{v}) = 0 \tag{1}$$

$$\frac{d\boldsymbol{v}}{dt} + \frac{1}{\rho}\nabla(P_{\rm i}+P_{\rm e}) = \boldsymbol{g} + \boldsymbol{f}_{\rm rad} \tag{2}$$

$$\frac{dP_{\rm i}}{dt} + \gamma\frac{P_{\rm i}}{\rho}\frac{d\rho}{dt} = -(\gamma-1)\,(\Lambda_{\rm ei}+\Lambda_{\rm h}) \tag{3}$$

$$\frac{dP_{\rm e}}{dt} + \gamma\frac{P_{\rm e}}{\rho}\frac{d\rho}{dt} = (\gamma-1)\,[\Lambda_{\rm ei}+\Lambda_{\rm h}-\nabla\cdot(\boldsymbol{q}+\boldsymbol{F}_{\rm rad})]\,. \tag{4}$$

Here, $\frac{d}{dt} = \frac{\partial}{\partial t} + \boldsymbol{v}\cdot\nabla$, $\rho = m_{\rm u}n_{\rm i}$ is the mass density with $m_{\rm u}$ the unit mass ($\simeq$ proton mass), and $\gamma = 5/3$ is the adiabatic index. On the right hand sides, the equation of motion contains the gravity $\boldsymbol{g}$ and the volume force exerted by absorbed and scattered radiation, $\boldsymbol{f}_{\rm rad}$. The latter becomes important when the accretion rate approaches the Eddington limit. In the energy equations, $\Lambda_{\rm ei}$ describes the energy exchange between ions and electrons by Coulomb collisons and $\Lambda_{\rm h}$ refers to electron heating by any other process, with the energy provided again by the ions. Additional energy gains of the electrons are described by the divergence of the heat conduction flow $\boldsymbol{q}$ and of the radiative flux $\boldsymbol{F}_{\rm rad}$. Calculation of the radiative flux (Eq. 5) requires solution of the radiative transfer equation (6) for the intensity $I_\nu(\boldsymbol{n},\nu)$ as a function of the direction $\boldsymbol{n}$ and the frequency ν, where σ and χ are the scattering and absorption coefficients, J_ν is the angle-averaged intensity and the use of B_ν for the source function indicates the assumption of LTE:

$$\boldsymbol{F}_{\rm rad} = \int_0^\infty \oint_{4\pi} I_\nu\, \boldsymbol{n}\, d\omega\, d\nu, \tag{5}$$

$$\boldsymbol{n} \cdot \nabla I_\nu = -(\sigma + \chi) I_\nu + \chi B_\nu + \sigma J_\nu . \tag{6}$$

Unsurprisingly, Eqs. (1)–(6) have not been solved in all their beauty, but only after the introduction of some rather severe simplifications.

4.2. Simplified Geometry

The correct funnel geometry (see Canalle, this conference) is most complicated to solve; the spherical or the linear geometry represent the simpler cases of which the latter is an acceptable approximation only for shock heights $h_{\rm sh} \ll R_{\rm wd}$. Realistic columns are always limited in the direction perpendicular to the flow. This limitation is of no concern when the radiative losses can be treated as optically thin emission, but in the optically thick case it requires a multi-dimensional radiative transfer (i.e., with the *direction* of $\nabla T_{\rm e}$ position-dependent). Comparatively simple cases are (i) a shallow infinite layer with the radiative flux vector constantly pointing in the radial direction (Woelk & Beuermann 1996, Fischer & Beuermann 2001) or (ii) a tall column with the radiative flux vector pointing only sideways (Cropper et al. 1999). Naturally, gravity effects increase with column height.

4.3. Electron Heating by Non-Coulomb Processes

In Eqs. (3) and (4), the quantity $\Lambda_{\rm h}$ represents any heating process other than Coulomb collisions. Non-Coulomb heating of electrons is known to occur in interplanetary shock fronts, in particular, the bow shock of the Earth (e.g. Stone & Tsurutani 1985). In these collisionless shocks (with a typical particle density of $n \sim 10\,{\rm cm}^{-3}$) characteristic processes are the reflection of ions, charge separation between electrons and ions, and the incidence of various types of plasma instabilities which lead to rapid electron heating. Plasma instabilities may also play a role in heating the electrons in supernova shocks (Lesch 1990). Whether such processes occur in MCV shocks with $\boldsymbol{v} \parallel \boldsymbol{B}$, high Mach numbers, and high particle densities (exceeding those in interplanetary space by factors of 10^{11} to 10^{16}) needs to be studied. Some authors (e.g. Saxton & Wu 2001) assume the presence of plasma heating in the shock front and consider $T_{\rm e}$ immediately behind the shock a free parameter, possibly ranging up to $T_{\rm i}$. Others, like Woelk & Beuermann 1992, 1996) and Fischer & Beuermann (2001) have disregarded plasma heating and considered Coulomb collisions only ($\Lambda_{\rm h} = 0$). In their solutions, the ion temperature displays a (quasi-)discontinuity at the shock, while the electron temperature increases only on a length scale which equals the Coulomb time scale times the flow speed. Clearly, the question of plasma heating in the shock front needs further consideration.

4.4. One-fluid Plasma

Electron and ion temperatures will be similar if the time scale for energy exchange between ions and electrons by Coulomb collisions is short compared with the cooling time scale. A one-fluid plasma is a reasonable approximation for high $\dot{m}$ and low B, while a two-fluid approach is required for low $\dot{m}$ and high B. The dividing line between the two regimes is approximately located at $\dot{m}B_7^{-2.6} \simeq 0.1$, where $\dot{m}$ is in $\mathrm{g\,cm^{-2}s^{-1}}$ and B_7 is in units of 10^7 G (see Fig. 4 below). Hence, $T_\mathrm{e} \simeq T_\mathrm{i}$ for $\dot{m}B_7^{-2.6} \gg 0.1$ and $T_\mathrm{e} < T_\mathrm{i}$ for $\dot{m}B_7^{-2.6} \ll 0.1$.

4.5. Cooling functions

The free-free optical depth of the post-shock flow parallel to $\boldsymbol{v}$ is $\tau_\mathrm{ff} \simeq 0.1 \ldots 1.0$. Hence, a flow cooling by bremsstrahlung only is optically thin to a first approximation with $\nabla \cdot \boldsymbol{F}_\mathrm{rad} = 1.4 \times 10^{-27} n_\mathrm{e}^2 T_\mathrm{e}^{1/2}\,\mathrm{erg\,cm^{-3}s^{-1}}$. In this case, the divergence term is a locally defined quantity which obviates the need for solving the radiative transfer equation. Most authors have simplified the radiative transfer by replacing $\nabla \cdot \boldsymbol{F}_\mathrm{rad}$ by a generalized cooling function expressed as the sum of terms of the form $\rho^a T_\mathrm{e}^b \propto \rho^{a-b} P_\mathrm{e}^b$ with a, b fixed for each term. Bremsstrahlung is represented by $a = 2, b = 0.5$, cyclotron radiation by $a = 0.15, b = 2.5$ (Saxton & Wu 2001, and references therein). The concept of a cooling function is applicable in approximately the same limit as the one-fluid plasma, $\dot{m}B_7^{-2.6} \gg 0.1$ (see Fig. 4 below). This limitation applies to radiative transfer through the shock front. For tall columns which lose energy preferentially through their sides, cooling functions are applicable also for lower values of $\dot{m}B_7^{-2.6}$

4.6. Energy Transport by Conduction

The heat conduction flow, $\boldsymbol{q} \propto n_\mathrm{e} T_\mathrm{e}^{5/2} \nabla T_\mathrm{e}$, is of importance only in regions of high particle density, high electron temperature, and/or a large gradient of the latter, i.e. (i) in the transition between the cooling flow and the stellar atmosphere and (ii) in the shock front with the adjoining pre-shock flow (Imamura et al. 1987). Most attempts to solve Eqs. (1)–(6) proceed with $\boldsymbol{q} = 0$. Wu (2000) has summarized the effects of heat conduction in MCVs.

4.7. Atomic Line Emission

The post-shock region is optically thick for the stronger atomic emission lines, complicating their calculation. One may adapt a procedure known from stellar atmosphere research which involves two steps: (i) the temperature structure is calculated assuming continuum absorption and emission only; (ii) the emerging emission line fluxes are calculated using this temperature structure. Tennant et al. (1998) and Wu et al. (2001) have used a cooling function for step (i) and a simplified line transfer for step (ii). An accurate calculation of the line profiles and line intensities requires substantial effort.

5. Oscillatory Solutions and Linear Stability Analysis

Time-dependent solutions of the hydrodynamic equations can be used to study the stability of stationary solutions. The added complication of the time dependence is compensated for by the simplicity of the coolong function. The stability analysis proceeds by, e.g., (i) assuming small perturbations of the position of the shock front and of the plasma parameters, (ii) linearization, and (iii) analysis of the growth rates of the harmonics of the oscillations (Langer et al. 1982, Saxton & Wu 2001, Wu 2000 and references therein). The possible frequencies are the equivalent to the harmonic oscillations of a pipe which is open at one end.

Saxton & Wu (2001) confirm earlier findings that shocks cooling by bremsstrahlung only are unstable against oscillations, except possibly in the fundamental mode. Shocks dominated by cyclotron cooling, on the other hand, are stable in the fundamental and all reasonably occurring higher oscillation modes. This suggests that stationarity is a reasonable model assumption if cyclotron emission is the dominant cooling agent. The low-amplitude oscillations with periods of $\sim 1-3\,$s seen in several MCVs (e.g. Larsson 1982) probably originate from regions within the accretion spot which are dominated by bremsstrahlung.

Solutions of Eqs. (1)–(6) with a time-dependent mass flux $\dot{m}$ incident on the white dwarf do not exist to my knowledge.

6. Stationary Solutions with Cooling Function

With $\nabla \cdot F_{\rm rad} = \Lambda_{\rm c} \propto \rho^{\rm a-b} P^{\rm b}$ (or a sum of such terms), only the hydrodynamic equations have to be solved. In the stationary case for linear or spherical geometry, Eqs. (1)–(4) reduce to a system of coupled ordinary (though non-linear) equations, in which all plasma parameters depend only on the radial coordiate.

6.1. One-fluid Plasma

For a one-fluid plasma, $P = P_{\rm e} + P_{\rm i}$ and Eqs. (3) and (4) may be combined to a single energy equation. The linear case is simplest and applies if the shock height is $h_{\rm sh} \ll R_{\rm wd}$. With $f_{\rm rad} = 0$, $\Lambda_{\rm h} = 0$, $\boldsymbol{q} = 0$, $\gamma = 5/3$, $g \simeq$ const, $z = r - R_{\rm wd}$, and $v < 0$, the hydrodynamic equations reduce to

$$\frac{d}{dz}(\rho v) = 0 \tag{7}$$

$$v\frac{dv}{dz} + \frac{1}{\rho}\frac{dP}{dz} = -g \tag{8}$$

$$v\frac{dP}{dz} - \frac{5}{3}v\frac{P}{\rho}\frac{d\rho}{dz} = -\frac{2}{3}\Lambda_{\rm c}, \tag{9}$$

For the above cooling function $\Lambda_{\rm c}$, a closed-integral solution has been given Wu et al. (1994). Because of the one-fluid assumption, the solution is limited to the high $\dot{m}$, low B part of the $\dot{m}$–B plane. In the spherical case, the mass flux ρv in Eq. (7) and g in Eq. (8) are r-dependent. The linear and spherical cases can be solved analytically if cooling is by bremsstrahlung only (Aizu 1973).

A potentially important case is that of a narrow, tall column (width $\ll$ height $\ll R_{\rm wd}$) which emits cyclotron radiation primarily sideways ($\perp B$). The radiative flux vector is then approximately in the x,y-plane which effectively decouples hydrodynamics and radiative transfer. With certain simplifying assumptions on the transverse radiative transfer, the radiative losses can be approximated by a cooling function (Wu et al. 1994, Cropper et al. 1999).

6.2. Stationary Two-fluid solution

For strong cyclotron cooling ($\dot{m}B_7^{-2.6} \ll 0.1$), the one-fluid approximation becomes invalid. Electron and ion temperatures differ, and Eq. (9) has to be replaced by

$$v\frac{dP_{\rm i}}{dz} - \frac{5}{3}\,v\,\frac{P_{\rm i}}{\rho}\frac{d\rho}{dz} = -\frac{2}{3}\left(\Lambda_{\rm ei} + \Lambda_{\rm h}\right) \tag{10}$$

$$v\frac{dP_{\rm e}}{dz} - \frac{5}{3}\,v\,\frac{P_{\rm e}}{\rho}\frac{d\rho}{dt} = \frac{2}{3}\left(\Lambda_{\rm ei} + \Lambda_{\rm h} - \Lambda_{\rm c}\right). \tag{11}$$

Although the temperatures deduced this way will be more reliable, the question of electron heating in the shock ($\Lambda_{\rm h}$) implies a remaining uncertainty. Temperature profiles of ions and electrons with different assumptions on $\Lambda_{\rm h}$ (and $\rho_{\rm o}$) are depicted, e.g., in Saxton & Wu (2001, their Fig. 3). For strong heating, the profiles are characterized by a maximum at the shock and a rapid decrease thereafter, while weak shock heating causes the electron temperature to assume a maximum further downstream, approaching the case of pure Coulomb heating.

7. Stationary Plane-parallel Two-fluid Radiation-hydrodynamics

The only truely radiation-hydrodynamic solution is that of Woelk & Beuermann (1996). Fischer & Beuermann (2001) present further results including a parametrization of the temperature profiles.

Their approach involves the solution of the four hydrodynamic equations, Eqs. (7), (8), (10), and (4) with $\Lambda_{\rm h} = 0$ and $q = 0$

$$v\frac{dP_{\rm e}}{dz} - \frac{5}{3}\,v\,\frac{P_{\rm e}}{\rho}\frac{d\rho}{dz} = \frac{2}{3}\left(\Lambda_{\rm ei} - \frac{dF_{\rm rad}}{dz}\right), \tag{12}$$

simultaneous with the radiative transfer equations (5) and (6). The solution of the latter was developed from a Feautrier code for plane-parallel stellar atmospheres, modified to include the anisotropy of cyclotron absorption and emission. The radiative transfer is fully frequency and angle dependent. The solution is energy conserving and ensures that the radiative flux (Eq. 6) exactly equals the accretion energy $\frac{1}{2}\dot{m}v_{\rm o}^2$. However, because of the plane-parallel ansatz the radiative flux is directed radially. In his review, Wu (2000) incorrectly states that the diffusion approximation was used and that energy is not conserved.

The solution relates $T_{\rm e}$ in a unique way to $\dot{m}$, B, and $M_{\rm wd}$ as the physical input parameters. Fig. 2 shows examples of the profiles of $T_{\rm e}(z)$, $T_{\rm i}(z)$, and $v(z)$ for $B = 30\,$MG and $\dot{m} = 0.01, 0.1$ and $1.0\,{\rm g\,cm^{-2}s^{-1}}$. Electron and ion temperatures are found to differ substantially near the shock front and equilibrate only further downstream. All flows are optically thick in the cyclotron fundamental which requires a negative electron temperature gradient to allow the energy to escape through the shock front. This is a consequence of the assumption of an *infinite* layer and may no longer hold true for columns of finite width. The effect of plama instabilities heating the electrons in the shock has not so far been considered by us and one can only speculate as to the effect they may have in the presence of optically thick radiative transfer. If the radiation escapes through the shock front, radiative transfer is likely to counteract plasma heating

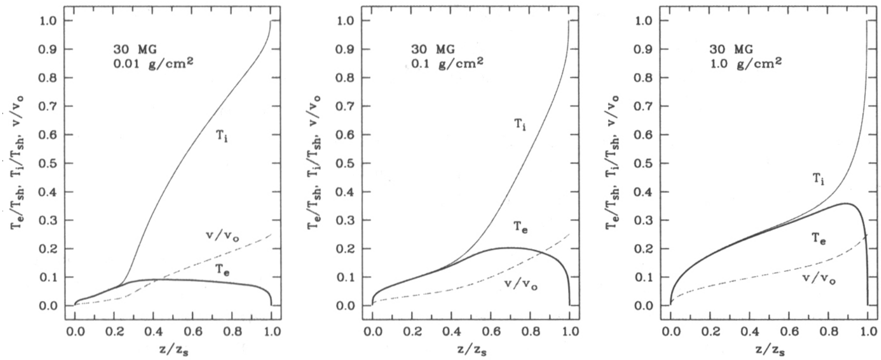

Figure 2. Profiles of $T_{\rm i}$, $T_{\rm e}$, and v for $B = 30\,\rm MG$, and $\dot m = 0.01$, 0.1, and $1.0\,\rm g\,cm^{-2}s^{-1}$ (from Fischer & Beuermann 2001).

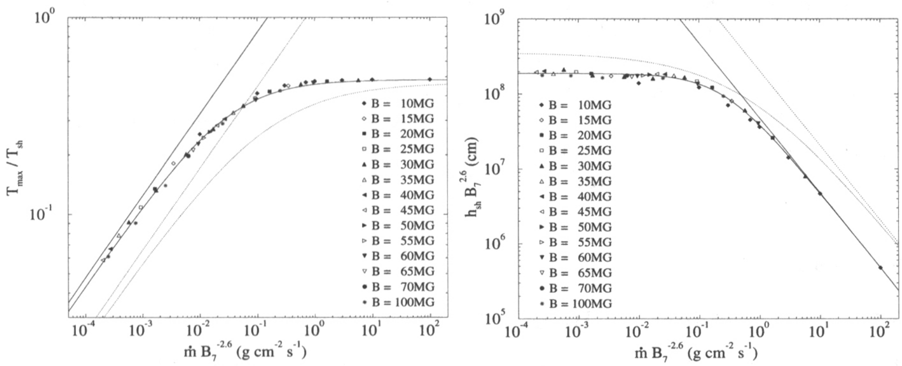

Figure 3. *(a) Left:* Peak electron temperature in units of the ion temperature at the shock for various values of the field strength vs. $\dot m B_7^{-2.6}$. *(b) Right:* Normalized shock height $h_{\rm sh} B_7^{2.6}$ vs. $\dot m B_7^{-2.6}$. See text for details.

and will tend to depress $T_{\rm e}$. I consider it unlikely that $T_{\rm e}$ at the shock can be anything near the Rankine-Hugoniot temperature for high B and low $\dot m$. The low temperatures of $\sim 1\,\rm keV$ observed from some AM Her stars (e.g. Schwope, this conference) seem to support this conclusion, but it is fair to state that the importance of plasma instabilities in MCV shocks is far from understood and further study is needed.

In Fischer & Beuermann (2001), we have parameterized the profiles $T_{\rm e}(z)$ by their peak value $T_{\rm max}$ and the shock height $h_{\rm sh}$. Fig. 3 shows $T_{\rm max}$ normalized to the ion temperature at the shock which initially contains all the energy (left panel) and a normalized version of the shock height (right panel). Both representations unify the results for a large range of model parameters ("data" points) into a unique dependence on the quantity $\dot m B_7^{-2.6}$ ("data" points and solid curves for $0.6\,\rm M_\odot$, dotted curves for $1\,\rm M_\odot$). It is noteworthy that the decreasing peak electron temperature for low $\dot m B^{-2.6}$ merges into the results for

https://doi.org/10.1017/S0252921100002098 Published online by Cambridge University Press

the bombardment solution (straight lines). In the same limit, the normalized shock height $h_{\rm sh}B_7^{2.6}$ (in cm) becomes constant. From Fig. 3 (right panel) one finds a limiting shock height for the $0.6\,{\rm M}_\odot$ white dwarf and for low $\dot{m}B^{-2.6}$ of $h_{\rm sh} \simeq 1.9 \times 10^8\,B_7^{-2.6}$, i.e. 10^7 cm for 30 MG and as low as 5×10^5 cm for 100 MG. Since bremsstrahlung-dominated shocks at the same B but higher $\dot{m}$ will be still lower, the assumption of plane-parallel or pillbox-shaped shocks is likely to be good for the higer field strengths.

In an attempt to generalize the results for a finite column width D, we have calculated the additional energy losses by optically thick radiation leaving their sides using a ray tracing technique (Fischer & Beuermann 2001). For a given $\dot{m}$, these added losses cause the equilibrium temperature to be *lower* than in an *infinite* layer. A correct treatment of the problem would require a truely 2-D radiative transfer which presents a substantial complication and introduces the width D as an additional model parameter besides $\dot{m}$. No such calculations are available in the literature. Fischer & Beuermann suggest a simple correction which ensures energy conservation: the electron temperature derived for $\dot{m}_\infty$ for an infinite layer approximately applies to the higher value $\dot{m}_{\rm D} = r\dot{m}_\infty$ for finite D, where $r = \mathcal{L}/\dot{m}v_{\rm o}$ is the ratio of the total radiative loss from the finite region over the accretion energy (both per cm^2). They provide a calibration of r as a function of $h_{\rm sh/D}$ and $\dot{m}B^{-2.6}$. Finally, note that in *all* models which approximate the optically thick radiative transfer by an emergent Planck spectrum cut off at some critical frequency ν^* energy is, by definition, only approximately preserved.

8. Applications

8.1. Free-standing vs. Buried Shocks

The ram pressure $P_{\rm ram} = \rho_{\rm o}v_{\rm o}^2$ of the infalling matter suppresses the bottom of the cooling flow into the atmosphere of the white dwarf. If also the shock front is located within the atmosphere, the shock is considered submerged or buried (Frank et al. 1988). Fig. 4 compares $h_{\rm sh}$ vs. $\dot{m}$ (from Fig. 3, right panel) to the depression produced by $P_{\rm ram}$. one finds that bremsstrahlung-dominated shocks are buried for $\dot{m} \gtrsim 10\,{\rm g\,cm^{-2}}$, while cyclotron-dominated shocks in high-field polars may be buried for much lower $\dot{m}$. To be sure, the chance for the upward directed radiation to escape will depend on the details of the geometry.

8.2. Emerging spectra as a function of $\dot{m}$

We have employed a heuristic model to estimate the effect of buried shocks on the emerging spectra. Specifically, we use a field strength of $B = 14$ MG (appropriate for AM Herculis) and consider radiation emerging at an angle against the radial direction of 60°. We consider subcolumns with $\dot{m}$ values ranging from 10^{-3} to $100\,{\rm g\,cm^{-2}s^{-1}}$, disregard the radiative interaction of the subsolumns, adopt a warm absorber which leaves soft X-rays largely unaffected, and approximately account for photoelectric absorption in the surrounding atmosphere using a ray tracing technique. Radiation intercepted by the white dwarf atmosphere is assumed to be reprocessed into UV radiation and soft X-rays with a temperature at the base of the individual subcolumns and their surroundings, which depends

https://doi.org/10.1017/S0252921100002098 Published online by Cambridge University Press

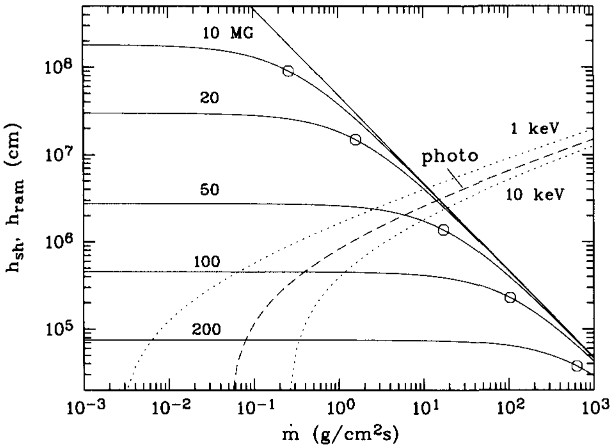

Figure 4. Shock height vs. mass flux $\dot{m}$ for a white dwarf mass of $0.6\,M_\odot$ and five values of the polar field strength. Also shown is the depression of the bottom of the post-shock flow below the photosphere (photo) and the level in the undisturbed atmosphere which corresponds to optical depths $\tau = 1$ for 1 keV and 10 keV photons.

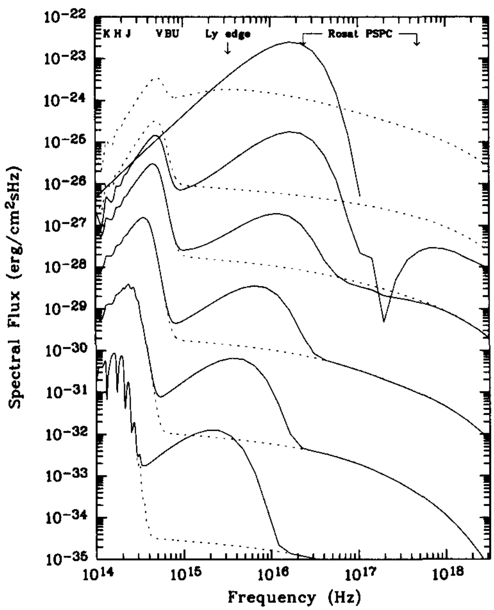

Figure 5. Representative emerging spectra for $B = 14\,$MG, $\Theta = 60°$ against the field direction, and mass fluxes $\dot{m} = 10^{-3}, 10^{-2}, 10^{-1}, 1, 10$, and $100\,\mathrm{g\,cm^{-2}s^{-1}}$, each for an emitting area of $10^{15}\,\mathrm{cm}^2$ at 100 pc distance. Dashed curves are the emitted spectra, solid curves the emerging spectra. The blackbody assumption is a crude approximation, in particular for the heated white dwarf at low $\dot{m}$.

https://doi.org/10.1017/S0252921100002098 Published online by Cambridge University Press

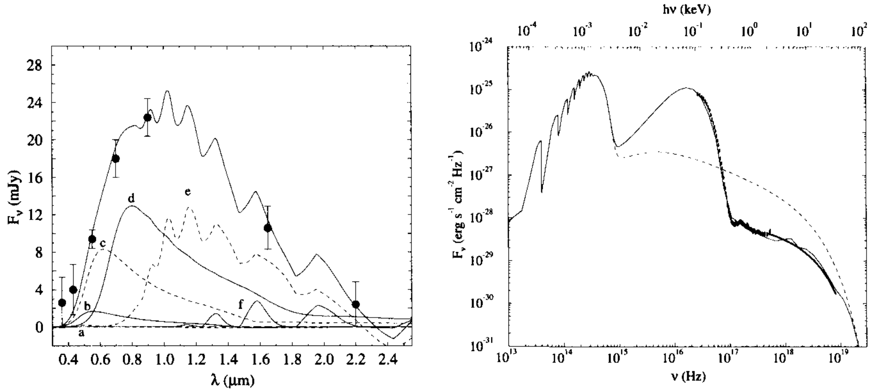

Figure 6. *(a) Left:* Synthesis of optical/IR cyclotron fluxes of AM Her in its high state (Priedhorsky et al. 1978). *(b) Right:* Synthesis of ROSAT X-ray spectrum (Gänsicke et al. 1995) extended to higher photon energies by the HEAO-1 spectrum (Rothschild et al. 1981

on the energy flux incident on the white dwarf. For simplicity, we assume blackbodies for the reprocessed flux. This assumption may be acceptable for the hot sections of the atmosphere, but the cooler UV emitting parts of the heated pole cap would correctly show the Lyman edge in absorption (Gänsicke et al. 1998, Fig. 12). In Fig. 5, the original emission and the reprocessed spectra are shown as dashed and solid curves, respectively. For low $\dot{m}$, the shock stands above the atmosphere and the emitted radiation escapes more or less freely, for larger $\dot{m}$ the originally emitted radiation is increasingly absorbed and reprocessed into soft X-rays, until at $\dot{m} = 100\,\mathrm{g\,cm^{-2}s^{-1}}$ the emission region is hidden behind an average column density of $\sim 10^{25}\,\mathrm{g\,cm^{-2}}$ and is completely reprocessed.

8.3. Spectral synthesis of AM Herculis

The characteristic shapes of the spectra in Fig. 5 depend on $\dot{m}$ and B. For a given field strength, such set of spectra can be used to synthesize the observed spectral energy distribution and thus yield the generating $\dot{m}$-distribution. Fig. 6 shows the result for AM Herculis, based on the cyclotron and X-ray spectral energy distributions observed near the respective orbital maxima. The cyclotron flux (Priedhorsky et al. 1978) is modelled by contributions with $100\,\mathrm{g\,cm^{-2}s^{-1}}$ (curve a) to $\dot{m} = 10^{-3}\,\mathrm{g\,cm^{-2}s^{-1}}$ (curve f), with very small contributions for $\dot{m} \gtrsim 3\,\mathrm{g\,cm^{-2}s^{-1}}$. The hard X-ray spectrum, on the other hand, originates mostly from mass fluxes around $1\ \mathrm{g\,cm^{-2}s^{-1}}$, and the large soft X-ray flux is produced by $\dot{m} \gtrsim 10\,\mathrm{g\,cm^{-2}s^{-1}}$. Hence, the origin of the individual contributions is to a sufficient extent mutually exclusive. It is comforting and adds to the credibility of the result that the contributions for $\dot{m}$ around $1\ \mathrm{g\,cm^{-2}s^{-1}}$ derived from the cyclotron and X-ray fluxes are consistent with each other. The same analysis has been performed for the low state of AM Herculis, using the infrared cyclotron spectrum of Bailey et al. (1991) and the low-state ROSAT PSPC spectrum of September 1991.

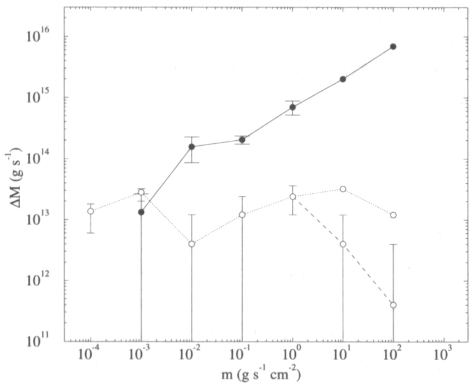

Figure 7. Contributions $\Delta\dot{M}$ to the accretion rate $\dot{M}$ from mass fluxes $\dot{m}$ between 10^{-4} and $100\,\mathrm{g\,cm^{-2}s^{-1}}$ for AM Herculis in its high state (filled circles) and its low state (open circles).

8.4. Distribution of Mass Fluxes in the Spot on AM Herculis

Figure 7 depicts the contributions $\Delta\dot{M}$ to the total time-averaged $\dot{M}$ in AM Her in its high state as derived from the spectra in Fig. 6. Also shown is the result of a corresponding analysis of the low state. While the errors in the derived values of $\Delta\dot{M}$ are much larger in the low state, a plausible picture emerges. The high state is characterized by a large contribution from high $\dot{m}$ which are largely missing in the low state, while a drizzle of low $\dot{m}$ seems to be present at all times (including most low states observed so far). Quite possibly, these differences exist already in the flow passing through the nozzle in L_1. Note that "$100\,\mathrm{g\,cm^{-2}s^{-1}}$" is actually a synonym for dense blobs since we are not able to distinguish between more or less dense blobs. The fate of blobs of different density is not considered here as long as the shocks are likely to be buried (compare Frank et al. 1988).

8.5. Variation of Hard vs. Soft X-rax Fluxes

It is long known that soft X-ray emission does not prevail in all AM Her stars, a notable exception being some systems with a low polar field strength (Beuermann & Schwope 1994, Ramsay et al. 1994, Ramsay this conference). One possible explanation is the shift of the whole $\dot{m}$-distribution towards smaller $\dot{m}$, which is expected to occur in systems with lower field strengths (Beuermann 1998).

9. Outlook

An attempt to model the entire internal structure of the emission spots in polars is probably futile. Some important aspects of the relevant physics need additional attention, however. Among them are the possible heating of electrons by plasma instabilities in MCV shocks, the effect of the optically thick radiative transfer on T_e, and the further development of two-fluid models. Pioneering studies of two-dimensional radiative transfer may be enlightening, too.

https://doi.org/10.1017/S0252921100002098 Published online by Cambridge University Press

On the observational side, studies high time resolution with the large ground-based and space-borne telescopes will undoubtedly provide a rapidly increasing insight into the dynamics and the spatial structure of the cyclotron as well as the X-ray emission regions.

References

Aizu, K. 1973, Prog. Theor. Phys., 49, 1184

Beuermann, K., & Schwope, A. D. 1994, ASP Conf. Ser., 56, 119

Beuermann, K. 1998, in TATA Golden Jubilee Conf. High Energy Astronomy and Astrophysics, p. 100, eds. P. C. Agrawal & P. R. Visvanath

Cropper, M., Wu, K., Ramsay, G., & Kocabiyik, A. 1999, MNRAS, 306, 684

Bailey, J., Ferrario, L., & Wickramasinghe, D. T. 1991, MNRAS, 251, 37p

Fischer, A., & Beuermann, K. 2001, A&A, 373, 211

Frank, J., King, A.R., & Lasota, J.-P. 1988, A&A, 193, 113

Gänsicke, B. T., Beuermann, K., de Martino, D. 1995, A&A, 303, 127

Gänsicke, B. T., Hoard, D.W. Beuermann, K., et al. 1998, A&A, 338, 933

Hameury, J.-M., & King, A. R. 1988, MNRAS, 235, 433

Imamura, J. N., Durison, R. H., Lamb, D. Q., Weast, G. J. 1987, ApJ, 313, 298

Lamb, D. Q., & Masters, A. R., ApJ, 234, L117

Langer, S. H., Chanmugam, G., & Shaviv, G. 1982, ApJ, 258, 289

Larsson, S. 1992, A&A, 265, 133

Lesch, H. 1990, A&A, 239, 437

King, A. R., & Lasota, J.-P. MNRAS, 188, 653

Kuijpers J., & Pringle J. E. 1982, A&A 114, L4

Priedhorsky, W., Matthews, K., Neugebauer, G., Werner, & M., Krzeminski, W. 1978, ApJ, 226, 397

Ramsay, G., 1994, MNRAS, 270, 692

Rothschild, R. E., Gruber, D. E., Knight, F. K., et al. 1981, ApJ, 250, 723

Saxton, C. J., Wu, K. 2001, 324, 659

Stone, R. G., Tsurutani, B. T., eds. 1985, Collisionless Shocks in the Heliosphere: A Tutoral Review, Geophysical Monograph 34, American Geophysical Union, Washington, D.C.

Tennant, A. F., Wu, K., O'Dell, S. L., Weisskopf, M. C. 1998, PASA, 15, 339

Woelk, U., & Beuermann, K. 1992, A&A, 256, 498

Woelk, U., & Beuermann, K. 1993, A&A, 280, 169

Woelk, U., & Beuermann, K. 1996, A&A, 306, 232

Wu, K. 2000, Space Sci.Rev., 93, 611

Wu, K., Chanmugam, G., & Shaviv, G. 1994 ApJ, 426, 664

Wu, K., Cropper, M., & Ramsay, G. 2001 MNRAS, 327, 208

Zheleznyakov, V. V. 1983, Ap&SS, 97, 229